Two distinct ferredoxins are essential for nitrogen fixation by the iron nitrogenase in *Rhodobacter capsulatus*

Holly Addison,[1] Timo Glatter,[2] Georg K. A. Hochberg,[3,4] Johannes G. Rebelein[1,4]

AUTHOR AFFILIATIONS See affiliation list on p. 15.

ABSTRACT Nitrogenases are the only enzymes able to fix gaseous nitrogen into bioavailable ammonia and hence are essential for sustaining life. Catalysis by nitrogenases requires both a large amount of ATP and electrons donated by strongly reducing ferredoxins or flavodoxins. Our knowledge about the mechanisms of electron transfer to nitrogenase enzymes is limited: The electron transport to the iron (Fe)-nitrogenase has hardly been investigated. Here, we characterized the electron transfer pathway to the Fe-nitrogenase in *Rhodobacter capsulatus via* proteome analyses, genetic deletions, complementation studies, and phylogenetics. Proteome analyses revealed an upregulation of four ferredoxins under nitrogen-fixing conditions reliant on the Fe-nitrogenase in a molybdenum nitrogenase knockout strain, compared to non-nitrogen-fixing conditions. Based on these findings, *R. capsulatus* strains with deletions of ferredoxin (*fdx*) and flavodoxin (*fld, nifF*) genes were constructed to investigate their roles in nitrogen fixation by the Fe-nitrogenase. *R. capsulatus* deletion strains were characterized by monitoring diazotrophic growth and Fe-nitrogenase activity *in vivo*. Only deletions of *fdxC* or *fdxN* resulted in slower growth and reduced Fe-nitrogenase activity, whereas the double deletion of both *fdxC* and *fdxN* abolished diazotrophic growth. Differences in the proteomes of Δ*fdxC* and Δ*fdxN* strains, in conjunction with differing plasmid complementation behaviors of *fdxC* and *fdxN,* indicate that the two Fds likely possess different roles and functions. These findings will guide future engineering of the electron transport systems to nitrogenase enzymes, with the aim of increased electron flux and product formation.

IMPORTANCE Nitrogenases are essential for biological nitrogen fixation, converting atmospheric nitrogen gas to bioavailable ammonia. The production of ammonia by diazotrophic organisms, harboring nitrogenases, is essential for sustaining plant growth. Hence, there is a large scientific interest in understanding the cellular mechanisms for nitrogen fixation *via* nitrogenases. Nitrogenases rely on highly reduced electrons to power catalysis, although we lack knowledge as to which proteins shuttle the electrons to nitrogenases within cells. Here, we characterized the electron transport to the iron (Fe)-nitrogenase in the model diazotroph *Rhodobacter capsulatus*, showing that two distinct ferredoxins are very important for nitrogen fixation despite having different redox centers. In addition, our research expands upon the debate on whether ferredoxins have functional redundancy or perform distinct roles within cells. Here, we observe that both essential ferredoxins likely have distinct roles based on differential proteome shifts of deletion strains and different complementation behaviors.

N itrogenases are the only known enzymes to perform nitrogen fixation, the biological reduction of molecular nitrogen (N_2) to bioavailable ammonia (NH_3).

Nitrogenases are found in many microorganisms across the domains of bacteria to archaea (1). Catalysis by nitrogenases requires chemical energy in the form of ATP and low-potential electrons to reduce N_2. The optimal catalytic activity is shown in (1) (2):

$$N_2 + 8H^+ + 16MgATP + 8e^- \rightarrow 2NH_3 + H_2 + 16MgADP + 16P_i \qquad (1)$$
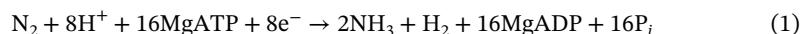
There are three known nitrogenase isoforms: the canonical molybdenum (Mo)-nitrogenase and two alternative nitrogenases, the vanadium (V)-nitrogenase and the iron (Fe)-nitrogenase (Fig. 1A). The isoforms are classified based on the differential metal composition of the cofactor present in the active site of the nitrogenase, although all three isoforms have a similar protein architecture, consisting of two reductase components and a catalytic component (3–5). Nitrogenases use metalloclusters for electron transfer through the components to the active site cofactor (Fig. 1B). Specifically, upon reduction by a single electron, the reductase component of nitrogenase binds two ATPs to subsequently form a complex with the catalytic component, where one electron is transferred from the $[Fe_4S_4]$-cluster to the P-cluster, an $[Fe_8S_7]$-cluster (6). The electrons flow through the catalytic component from the P-cluster to the active site metallocluster, where the reduction of N_2 occurs (7). ATP hydrolysis is believed to trigger the release of the reductase component from the catalytic component, with P_i release being the rate-limiting step (8). Despite similarities in the mechanisms of N_2 reduction by the different nitrogenases, the isoforms harbor differential side activities for reducing non-nitrogen substrates, such as CO_2 to short-chain hydrocarbons, that is, methane, ethene, and ethane (3, 9–12). Notably, the Fe-nitrogenase was shown to have the highest efficiency for reducing CO_2 compared to the other two nitrogenase isoforms (13, 14).

Despite extensive studies examining intramolecular electron transfer within a nitrogenase enzyme, there is relatively limited knowledge about the intermolecular electron transfer to the nitrogenases (7). Only electron transport to Mo-nitrogenases has been investigated previously in *Rhodobacterales* (19–22). The electron transport to either alternative nitrogenase (V- and Fe-nitrogenase) has not been investigated prior (23). Here we use the bacterium *Rhodobacter capsulatus* to investigate electron transport
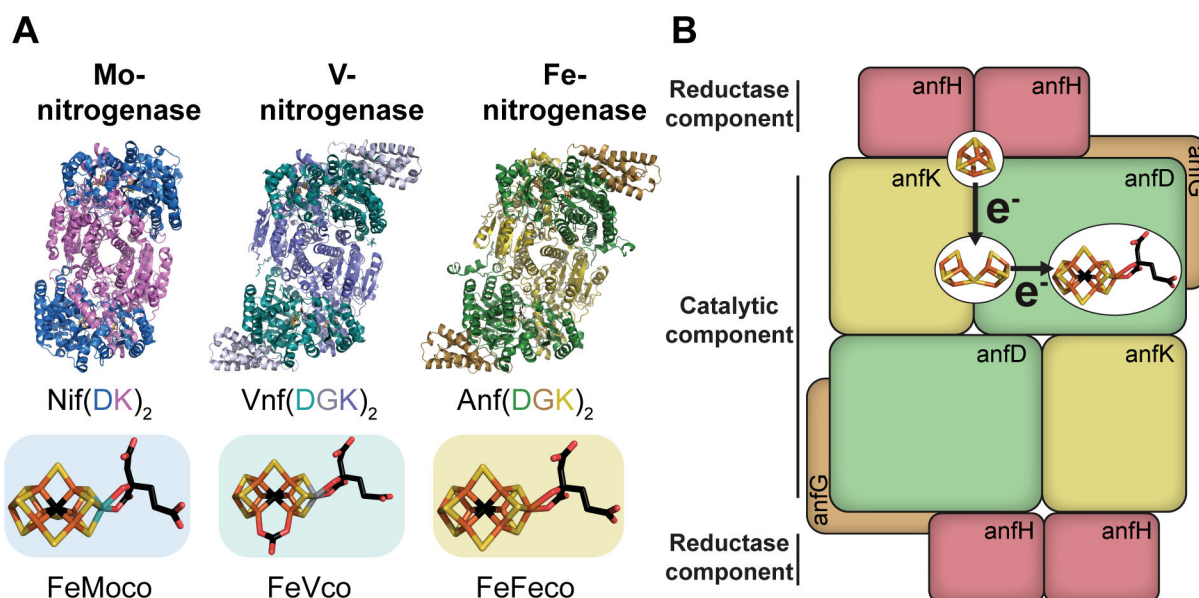

FIG 1 Overview of the three nitrogenase systems, cofactors, electron flow, and subunit interactions. (A) Structures of the catalytic components and active site cofactors of the three nitrogenase isoforms (15–18). Ribbon presentation of the three nitrogenase catalytic components with subunit annotation below. At the bottom are stick representations of the three active site metalloclusters in colored boxes. (B) Schematic of the electron transfer within the Fe-nitrogenase from the $[Fe_4S_4]$-cluster *via* the P-cluster to the FeFeco. Black arrows indicate the movement of a single electron. (A-B) The metalloclusters are shown as stick models with carbon in black, iron in orange, oxygen in red, sulfur in yellow, molybdenum in blue, and vanadium in gray.

to the alternative Fe-nitrogenase. As *R. capsulatus* only harbors Mo- and Fe- nitrogenases, the expression system is easier to engineer and results in a more robust expression of the Fe-nitrogenase compared to model diazotrophs which harbor all three nitrogenase isoforms, that is, *Azotobacter vinelandii* and *Rhodopseudomonas palustris* (24–26). A key route of electron transport to the Mo-nitrogenase in *R. capsulatus* which is also expected to be involved in electron transport to the Fe-nitrogenase is through the Rhodobacter Nitrogen Fixation complex (Rnf complex, Fig. 2). The six structural *rnf* genes are encoded within the N_2-fixation gene clusters and are known to be essential for N_2 fixation by the Mo-nitrogenase (27, 28). Under N_2-fixing conditions, the Rnf complex is expected to catalyze the reduction of ferredoxins (Fds), utilizing energy from a H^+ or Na^+ gradient while electrons are provided by the oxidation of NADH to NAD^+ (29). Both the identity of the electron acceptor for Rnf and the exact redox thermodynamics of Rnf catalysis in *R. capsulatus* remain unknown.

An ample supply of electrons from NADH is necessary for Rnf-mediated Fd reduction in *R. capsulatus*. A key generator of NADH in N_2-fixing *R. capsulatus* cells is complex I, the NADH:ubiquinone oxidoreductase. Under N_2-fixing conditions, complex I was shown to mediate reverse electron flow from the membrane quinone pool to reduce NAD^+ to NADH in the cytosol (30). Deletion of complex I resulted in unviable cells due to an imbalance in the cellular redox homeostasis. Thus, complex I is an essential route for electrons to pass to the Mo-nitrogenase, which is a key electron sink in *R. capsulatus* (30).

A second route of electrons to the Mo-nitrogenase involves the pyruvate-ferredoxin oxidoreductase (NifJ, Fig. 2) (31). NifJ reduces Fds or flavodoxins (Flds) while oxidizing pyruvate to acetyl-CoA in anaerobic carbon metabolism and is a critical component of the electron transport pathway to Mo-nitrogenase in other proteobacteria, such as *Klebsiella pneumoniae* (32). *R. capsulatus* NifJ is known to drive the Mo-nitrogenase *in vitro* when combined with purified *R. capsulatus* NifF (flavodoxin 1) (31).
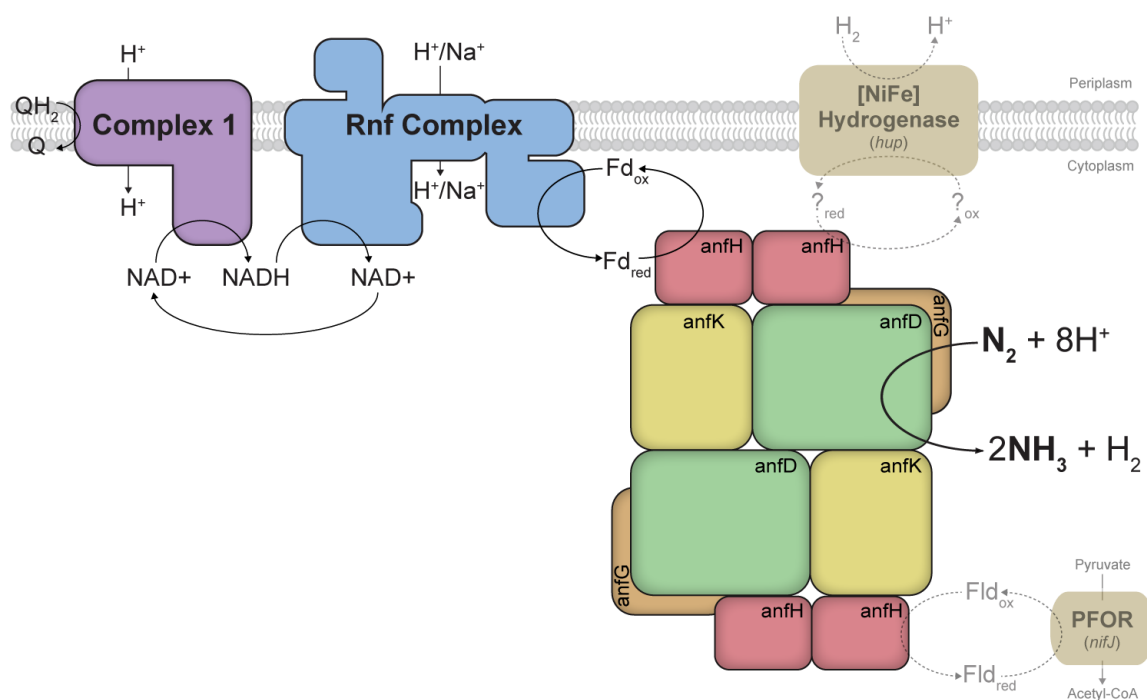

FIG 2 Overview of proposed electron transport routes to the Fe-nitrogenase in *R. capsulatus*. Black arrows indicate the believed prominent route of electrons to the Fe-nitrogenase in *R. capsulatus*. This flow of electrons toward the Fe-nitrogenase is through complex I, the Rnf complex, and a Fd of unknown identity. Electrons are believed to flow from the reduced quinone pool in the inner membrane through complex I onto NADH, after which Rnf oxidizes NADH to reduce Fd, the reductant of nitrogenase enzymes. Dashed and faint arrows indicate possible alternative electron transfer routes to the Fe-nitrogenase, specifically through the pyruvate:ferredoxin oxidoreductase (PFOR, *nifJ*) and the [NiFe] hydrogenase.

TABLE 1 Properties of ferredoxins and flavodoxin from *Rhodobacter capsulatus*[b]

Protein	Gene	Cofactor(s)	Donates electrons to Mo-nitrogenase *in vitro*
FdA (FdII)	*fdxA*[a]	$[Fe_4S_4]$- and $[Fe_3S_4]$-cluster	Yes (42)
FdB (FdIII)	*fdxB*	$2[Fe_4S_4]$-cluster	No (43)
FdC (FdIV)	*fdxC*	$[Fe_2S_2]$-cluster	ND
FdD (FdV)	*fdxD*	$[Fe_2S_2]$-cluster	No (44)
FdE (FdVI)	*fdxE*[a]	$[Fe_2S_2]$-cluster	ND
FdN (FdI)	*fdxN*	$2[Fe_4S_4]$-cluster	Yes (45)
NifF (FldI)	*nifF*	FMN	Yes (46)

[a]*fdx* genes could not be deleted from *R. capsulatus* as observed prior (40, 41).
[b]ND stands for not determined. Other commonly used protein abbreviations are shown in brackets.

Finally, the uptake [NiFe] hydrogenase HupAB (also called HupSL), which under diazotrophic conditions oxidizes H_2 to H^+, supports electron transport to nitrogenases (Fig. 2) (33). H_2 is the main byproduct of nitrogen reduction by nitrogenases and *R. capsulatus* is thought to recycle these lost electrons to drive nitrogenases (34, 35). However, the identity of the redox acceptor for the *R. capsulatus* [NiFe] uptake hydrogenase remains unclear. One suggestion is that electrons can move directly from [NiFe] hydrogenases into the ubiquinone pool, where other unknown oxidoreductases can reduce soluble charge carriers to reduce nitrogenases (36).

Soluble charge carriers typically perform the final electron transfer step to nitrogenase enzymes, specifically Fds or Flds (23). Fds contain redox-active Fe-S-clusters, whereas Flds use a flavin mononucleotide (FMN) as the redox cofactor (29). Known charge carriers to nitrogenases are strongly reducing, with very low reduction potentials, thereby allowing the reduction of the $[Fe_4S_4]$-cluster in the subunit interface of the nitrogenase reductase (37). There is considerable interest in the final step of electron delivery to nitrogenases, as it has been suggested to limit N_2 fixation *in vivo* (20, 38). Interestingly, Fds can have other roles in nitrogen fixation. Some Fds are involved in the maturation of nitrogenase cofactors, donating electrons to assembly proteins such as NifB (36, 37).

The genome of *R. capsulatus* contains genes for six Fds (*fdx*), four of which are located on the N_2 fixation gene clusters, and one Fld (NifF, Fld1), not encoded on the N_2 fixation gene clusters (24, 28, 39). Only two of the six Fds, FdA and FdE, are essential for *R. capsulatus* growth under non-diazotrophic conditions, shown by the inability to construct viable deletion mutants of the genes *fdxA* and *fdxE* (40, 41). It is unknown which electron carriers are relevant for supplying electrons to the Fe-nitrogenase in *R. capsulatus*, and other diazotrophs, *in vivo*. However, prior work has determined that FdA, FdN, and NifF can reduce the *R. capsulatus* Mo-nitrogenase *in vitro* (Table 1).

In this study, we characterize the electron transport to the Fe-nitrogenase for the first time. Our experiments show that the individual deletion of *fdxN* or *fdxC* decreases the Fe-nitrogenase-catalyzed N_2 fixation, while the double deletion of *fdxCN* abolishes N_2 fixation entirely. Next, we started to engineer the electron transport to the Fe-nitrogenase by re-introducing *fdxN* or *fdxC* on plasmids with different copy numbers under the Fe-nitrogenase promoter. *fdxN* complementation was tolerated from both single and high copy number plasmids. By contrast, *fdxC* complementation was only tolerated using a single copy number plasmid, while the high copy number plasmid abolished diazotrophic growth. This information, along with differential proteome shifts for Δ*fdxN* vs Δ*fdxC* strains, showed that FdN and FdC likely have specific roles in *R. capsulatus* and are not redundant in function. Our findings suggest that FdN and FdC have distinct functions in N_2 fixation, which could originate from the known structural and electrochemical differences (47).

RESULTS

We set out to identify which soluble charge carriers, that is, Fds or Flds in *R. capsulatus,* are associated with diazotrophic growth and N$_2$ fixation *via* the Fe-nitrogenase in a Mo-nitrogenase knockout strain (Δ*nifD,* Δ*modABC*); the wildtype (WT) strain used throughout the paper. To achieve this, we used whole-cell proteomics to compare protein abundances between *R. capsulatus* growth on NH$_4^+$ (non-N$_2$-fixing conditions), under which N$_2$ fixation genes are suppressed (48), and *R. capsulatus* growth with N$_2$ as the sole nitrogen source (N$_2$-fixing conditions) (Fig. 3).

As expected, most (44 of 56) N$_2$ fixation-related proteins were upregulated under N$_2$-fixing conditions (Fig. 3A), while 10 proteins remained similar, and only NifJ was downregulated (Tables S2 and S3). Unsurprisingly, some of the most highly upregulated proteins were Fe-nitrogenase subunits, as diazotrophically grown *R. capsulatus* strictly depends on nitrogenase activity for growth.

Several oxidoreductase proteins implicated in electron transport to nitrogenase were differentially produced under N$_2$-fixing conditions (Fig. 3B). Most notably, six of seven Rnf complex subunits were strongly upregulated (20, 27). The upregulation shows that Rnf production is linked to Fe-nitrogenase-mediated N$_2$ fixation and likely has a crucial role in supplying electrons for catalysis. Also, both the small and large subunits of the uptake hydrogenase HupAB had increased expression. HupAB upregulation aligned with prior studies showing increased HupAB activity when nitrogenase is active and producing H$_2$, compared to non-N$_2$-fixing conditions (NH$_4^+$) (33). Only NifJ was downregulated under N$_2$-fixing conditions, supporting prior studies that showed NifJ was produced at similar levels under both N$_2$-fixing and non-N$_2$-fixing conditions (31). NifJ downregulation
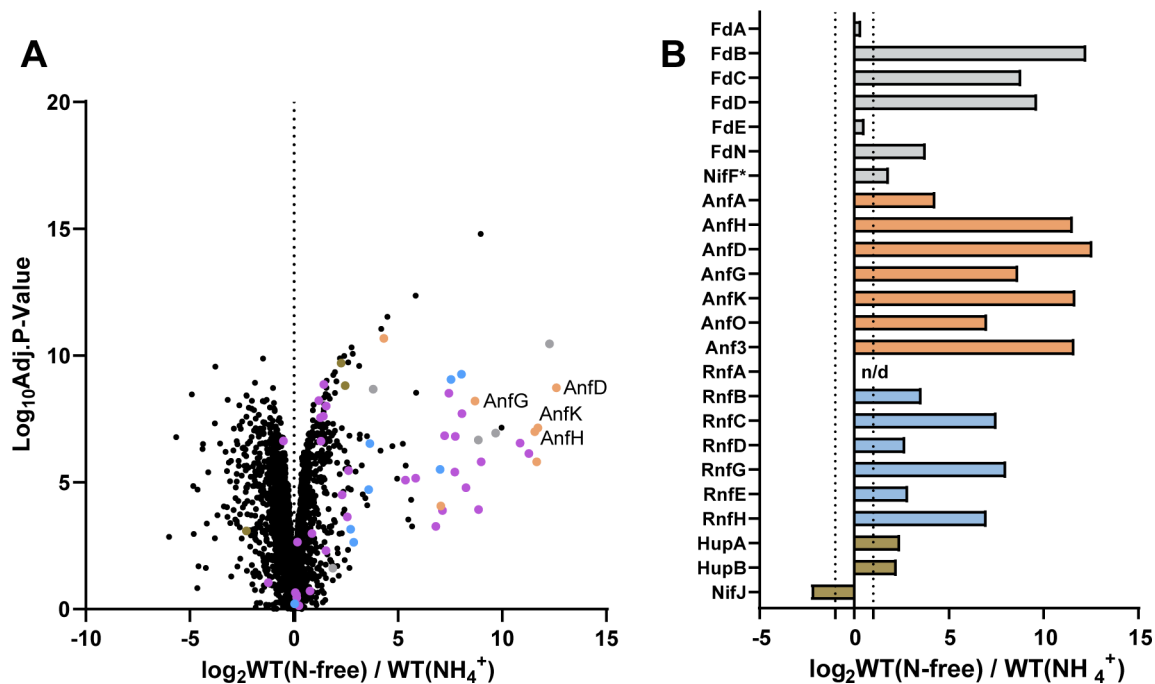

FIG 3 Upregulation of N$_2$ fixation proteins in *R. capsulatus* under diazotrophic growth. (A) Volcano plot displaying mean intensity log$_2$-ratios (X-axis) versus significance values (−log$_{10}$ adjusted P-values, Y-axis) of the changing proteome of *R. capsulatus* grown in N-free and NH$_4^+$-containing media. N$_2$ fixation-related proteins are highlighted. Fd and Fld proteins (gray), Fe-nitrogenase structural and associated proteins (Anf-proteins are labeled in orange), Rnf proteins (light blue), Hup proteins and NifF (brown), and other detected proteins encoded on the N$_2$ fixation gene clusters (28) (purple). (B) Bar chart displaying average mean intensity log$_2$-ratios of highlighted proteins between N$_2$-fixing conditions and non-N$_2$ fixing conditions. Proteins are color-coded as in (A). The dotted line indicates a log$_2$-fold-change of 1 and n/d stands for not detected. (A-B) All proteins with a log$_2$-fold-change of >±1 were considered up- or down-regulated between N$_2$-fixing conditions (WT (N-free)) and non-nitrogen fixing conditions (WT (NH$_4^+$)). All proteins with a 0.01 *P*-value (log$_{10}$Adj.*P*-Value over 2.0) were considered significant, starred proteins (*) did not meet significance criteria. The strain carries an in-frame deletion of Δ*nifD* Δ*modABC* to ensure the expression of Fe-nitrogenase genes (*anf*). Coefficients of variation between four independent cultures are provided in Table S2.

TABLE 2 Doubling times of *fdx* and *nifF* deletion mutants of *Rhodobacter capsulatus* strains[a]

Genotype	Doubling time (h)
WT	10.31 ± 0.8
$\Delta fdxB$	10.49 ± 1.5
$\Delta fdxC$	43.7 ± 21.2
$\Delta fdxD$	8.81 ± 0.6
$\Delta fdxN$	28.7 ± 4.4
$\Delta fdxCN$	>100
$\Delta nifF$	8.83 ± 0.5
$\Delta anfDGK$	>100

[a]An exponential Malthusian growth model was used to determine individual doubling times. Only OD_{660} values in the linear range were included. The means and standard deviation of the doubling times were calculated using three biological replicates.

implies that it may not be a vital contributor to reduced Fds for Fe-nitrogenase reduction under the tested conditions.

The soluble electron carriers FdC, FdB, FdD, and FdN were all significantly upregulated under N_2-fixing conditions (Fig. 3B). Notably, there was not a significant change in NifF (Fld1) expression under N_2-fixing conditions despite prior studies showing NifF to drive Mo-nitrogenase *in vitro* (46). The proteome analyses also revealed that the expression level of the essential FdA and FdE was almost constant under the tested conditions, suggesting these proteins may not have any additional role under diazotrophic conditions (40).
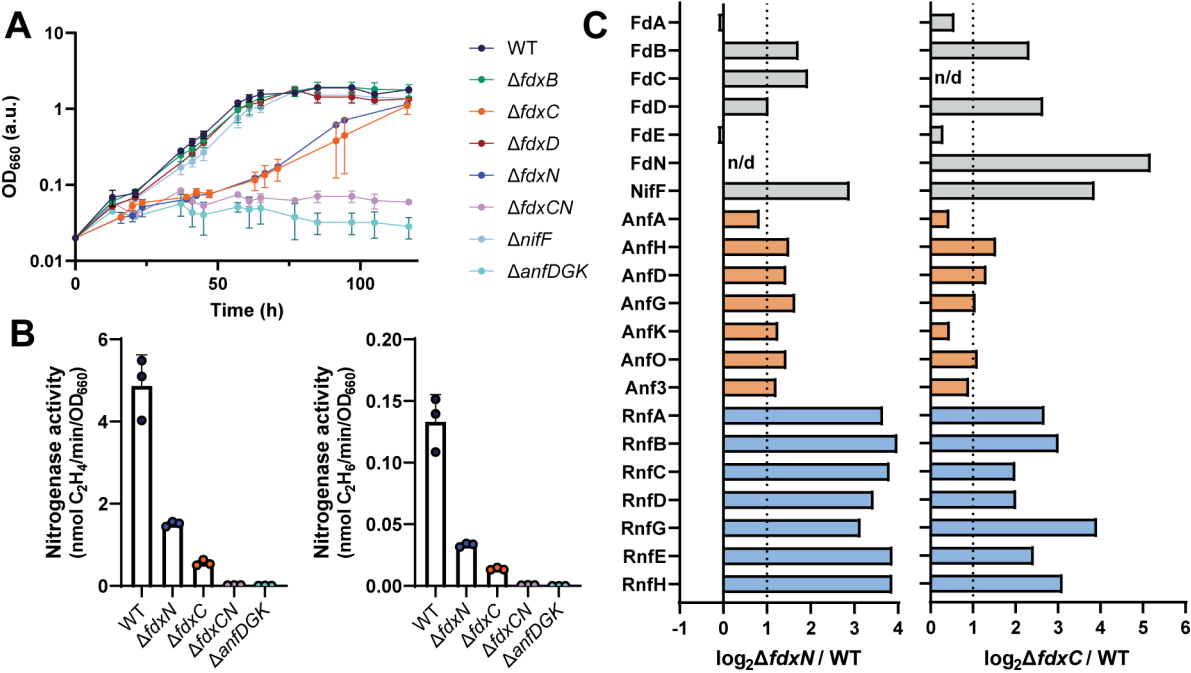

FIG 4 Deletion of *fdxN* and/ or *fdxC* impairs N_2 fixation by the Fe-nitrogenase in *R. capsulatus*. (A) Diazotrophic growth of *R. capsulatus* strains dependent on the Fe-nitrogenase. (B) Fe-nitrogenase activity determined *via* acetylene reduction by *R. capsulatus* strains. All strains, except those with no net OD_{660} increase ($\Delta fdxCN$, $\Delta anfDGK$) were normalized by final OD_{660}. (C) Bar chart displaying average mean intensity $\log_2$-ratios of highlighted proteins between $\Delta fdxN$ and WT (left) and $\Delta fdxC$ and WT (right). Fd and Fld proteins (gray), Fe-nitrogenase structural and associated proteins (Anf) (orange), and Rnf proteins (light blue). All proteins with a $\log_2$-fold-change of $>\pm1$ were considered up- or downregulated between $\Delta fdxN$ or $\Delta fdxC$ strains ($\Delta fdxN$ or $\Delta fdxC$) and the WT. The dotted line indicates a log-fold-change of 1 and n/d stands for not detected. All proteins with a 0.01 *P*-value ($\log_{10}$Adj.*P*-Value over 2.0) were considered significant. Coefficients of variation between four independent cultures are provided in Table S4. (A-B) Data are from three independent cultures; error bars represent the standard deviation from the mean. (A-C) All strains carry an in-frame deletion of $\Delta nifD$ $\Delta modABC$ to ensure the expression of Fe-nitrogenase genes (*anf*). *R. capsulatus* strains were grown diazotrophically in an RCV minimal medium under an N_2 atmosphere.

To evaluate the roles of every upregulated Fd under N_2-fixing conditions, each Fd was individually and scarlessly deleted from the genome of *R. capsulatus*. Diazotrophic growth was monitored *via* OD_{660} over time and Fe-nitrogenase activity by the acetylene reduction assay, releasing ethylene and ethane, measured during the exponential growth phase (Fig. 4A and B).

Deletion of *fdxN* or *fdxC* slowed diazotrophic growth by threefold to fourfold, with doubling times of 28.7 h for Δ*fdxN* and 43.7 h for Δ*fdxC* compared to 10.3 h for the wild type (Fig. 4A; Table 2). Deletion of both *fdxN* and *fdxC* in the same strain abolished diazotrophic growth by the Fe-nitrogenase, indicating a compounding of the growth issues when both genes are deleted. These results were corroborated by a decrease in Fe-nitrogenase activity of threefold to fourfold for the separate deletion strains Δ*fdxN* and Δ*fdxC* and no activity for the double Δ*fdxCN* deletion strain (Fig. 4B). These findings are in agreement with previous Mo-nitrogenase studies, which observed decreased Mo-nitrogenase activity and diazotrophic growth upon deletion of *fdxN* and/or *fdxC* (22, 41, 49).

All other deletion strains, Δ*fdxB*, Δ*fdxD*, and Δ*nifF*, had no diazotrophic growth defects. Thus, these genes are not essential for Fe-nitrogenase-mediated N_2 fixation under photoheterotrophic conditions, or their functions can be complemented by the remaining Fds/ Flds. Our results agree with previous findings for the Mo-nitrogenase, which showed that the interruption of *fdxD, fdxB,* and *nifF* did not affect Mo-nitrogenase-based diazotrophic growth (39, 43, 50). Potentially FdB, FdD, and NifF have redundant functions or only support Mo-nitrogenase activity. Moreover, FdD has been implicated in oxygen protection of the Mo-nitrogenase but not the Fe-nitrogenase (50).

Changes in the proteomes of the individual Δ*fdx* deletion strains were investigated to explore the possible roles of the *fdxN* and *fdxC* gene products, FdN and FdC, respectively. Whole proteome analysis revealed that the proteomes of the Δ*fdxN* and Δ*fdxC* deletion strains changed, relative to the WT under diazotrophic growth, to respond to the loss of one essential *fdx* gene (Fig. S1 and S2; Tables S4 and S5). There were significant changes in the abundance of soluble charge carriers in both Δ*fdxN* and Δ*fdxC* compared to WT (Fig. 4C). Specifically, the deletion of *fdxN* caused an upregulation of FdB, FdD, FdC and NifF. The same trend was observed for *fdxC,* though FdN was the most upregulated soluble charge carrier here, with NifF the second most. *In vitro* studies with the Mo-nitrogenase have shown that both FdN and NifF can donate electrons to the Mo-nitrogenase, although levels of FdN were much higher in cells (51, 52). Perhaps the cells are attempting to push electrons through an alternative electron carrier instead of Fds when *fdxN or fdxC* are removed.

The observed changes in the abundance of FdN in Δ*fdxC* and NifF in both Δ*fdxC* and Δ*fdxN* may represent a cellular response to overcome the deficits in N_2 fixation by upregulating the production of proteins capable of reducing the Fe-nitrogenase reductase. Notably, FdN has a $\log_2$-fold change of over five in Δ*fdxC*, revealing a reliance of the cells on FdN when FdC is absent. On the other hand, there was only a $\log_2$-fold change of 2 for FdC in Δ*fdxN*.

Many further proteins involved in N_2 fixation were upregulated in both the Δ*fdxN* and Δ*fdxC* strains, the most prominent being Rnf proteins (Fig. 4C). The upregulation of Rnf proteins supported prior work that showed the Rnf complex is the main route of electrons to Mo-nitrogenase in *R. capsulatus* (20). Interestingly, there was no significant change in the abundance of NifJ or HupAB in either Δ*fdxN* or Δ*fdxC* (Fig. S3). It appears that the primary response of the cells is to upregulate the Rnf pathway for electron transport.

Having successfully characterized the *fdx* deletion strains, we aimed to restore WT growth rates by complementing Δ*fdxN* and Δ*fdxC* with plasmids encoding *fdxN* or *fdxC* (Fig. 5 and 6). *fdxN* and *fdxC* were separately cloned into a high copy and a single copy plasmid, both under the control of the Fe-nitrogenase promoter (*anfH*), to test which conditions recovered N_2 fixation.
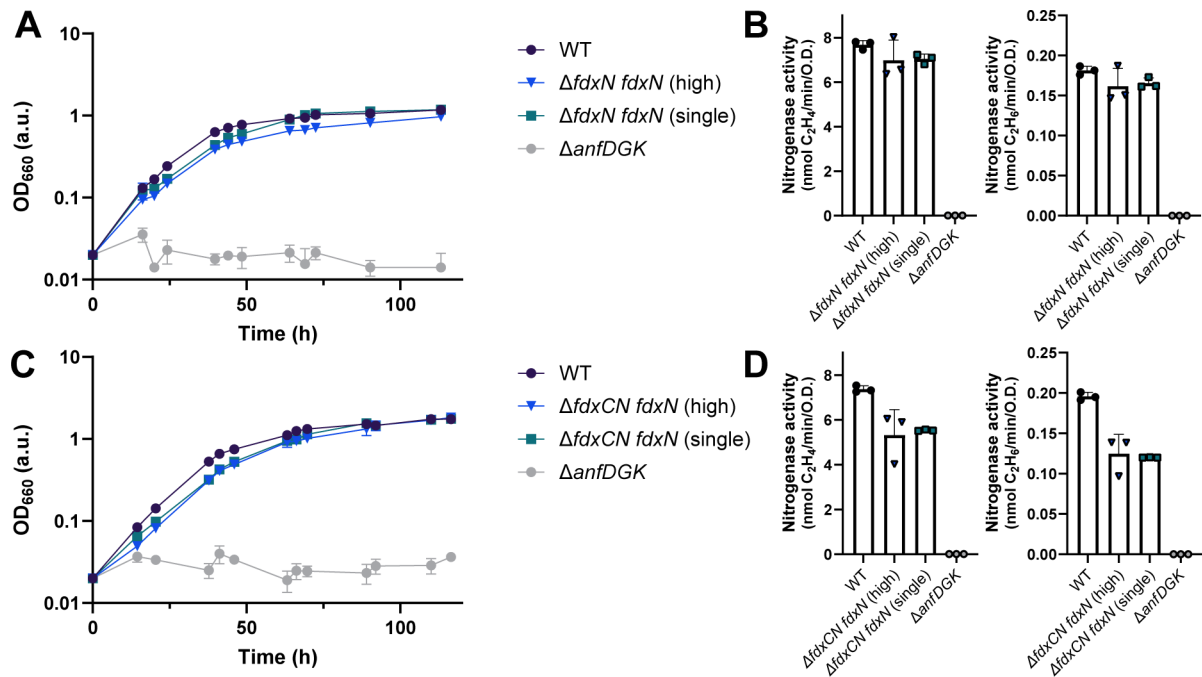
FIG 5 Complementation of *fdxN* recovers N₂ fixation by the Fe-nitrogenase in *R. capsulatus*. (A) Diazotrophic growth of the Δ*fdxN R. capsulatus* complementation strains with *fdxN* on high- and single-copy plasmids. (B) Fe-nitrogenase activity was determined *via* acetylene reduction by *R. capsulatus fdxN* complemented Δ*fdxN* strains. (C) Diazotrophic growth of the Δ*fdxCN R. capsulatus* complementation strains with *fdxN* on high- and single-copy plasmids. (D) Fe-nitrogenase activity was determined *via* acetylene reduction by *R. capsulatus fdxN* complemented Δ*fdxCN* strains. (B, D) All strains except those with no net OD₆₆₀ increase (Δ*anfDGK*) were normalized by final OD₆₆₀. (A-D) Data are from three independent cultures. Error bars represent the standard deviation from the mean. All strains carry an in-frame deletion of Δ*nifD* Δ*modABC* to ensure the expression of Fe-nitrogenase genes (*anf*). *R. capsulatus* strains were grown diazotrophically in an RCV minimal medium under an N₂ atmosphere.

Expression of *fdxN* under the *anfH* promoter from plasmids recovered diazotrophic growth in both the Δ*fdxN* and the Δ*fdxCN R. capsulatus* strains (Fig. 5A and C). Doubling times of all *fdxN* complementation strains were close to WT, even those in Δ*fdxCN* mutants, at around 10–11 h (Table 3). The doubling time of the Δ*fdxCN fdxN* strain was faster than the Δ*fdxC* strain, which also had one copy of *fdxN* and no copies of *fdxC* but a slower doubling time of around 30 h (Table 2). The faster growth of strain Δ*fdxCN fdxN* could be due to the strength of the *anfH* promoter compared with the *fdxN* native promoter in the genome (the *fprA* promoter). Differential promoter strengths could cause higher transcription rates of *fdxN* in the Δ*fdxCN fdxN* strain relative to the Δ*fdxC* strain, explaining the doubling time differences. Furthermore, FdN was the most

TABLE 3 Doubling times of *fdx* complemented *Rhodobacter capsulatus* strains[a]

Genotype	Doubling time (h)
WT	11.19 ± 0.7
Δ*fdxN fdxN* (high)	11.1 ± 0.1
Δ*fdxN fdxN* (single)	11.7 ± 0.7
Δ*fdxC fdxC* (high)	>100
Δ*fdxC fdxC* (single)	13.1 ± 1.0
Δ*fdxCN fdxN* (high)	10.77 ± 0.2
Δ*fdxCN fdxN* (single)	10.91 ± 0.3
Δ*fdxCN fdxC* (high)	>100
Δ*fdxCN fdxC* (single)	23.5 ± 3.0
Δ*anfDGK*	>100

[a]An exponential Malthusian growth model was used to determine individual doubling times. Only OD₆₆₀ values in the linear range were included. The means and standard deviation of the doubling times were calculated using three biological replicates.
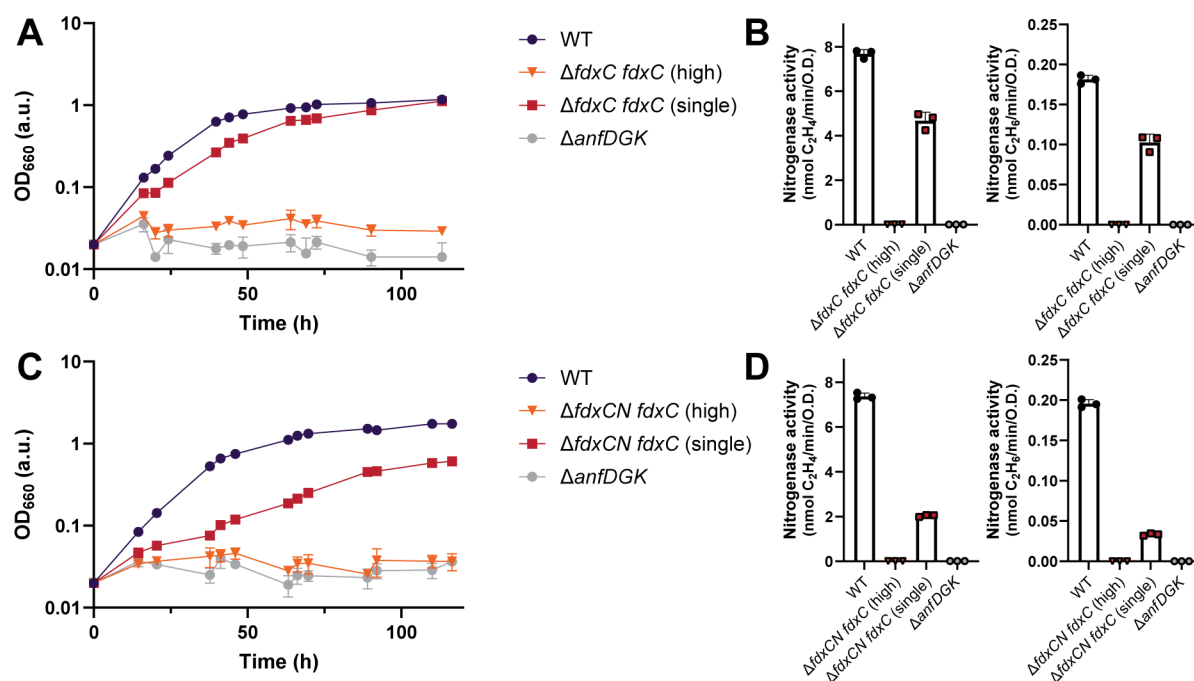
FIG 6 Complementation of *fdxC* on a single-copy plasmid recovers N_2 fixation by the Fe-nitrogenase in *R. capsulatus*. (A) Diazotrophic growth of the Δ*fdxC R. capsulatus* complementation strains with *fdxC* on high- and single-copy plasmids. (B) Fe-nitrogenase activity was determined *via* acetylene reduction by *R. capsulatus fdxC* complemented Δ*fdxC* strains. (C) Diazotrophic growth of the Δ*fdxCN R. capsulatus* complementation strains with *fdxC* on high- and single-copy plasmids. (D) Fe-nitrogenase activity was determined *via* acetylene reduction by *R. capsulatus fdxC* complemented Δ*fdxCN* strains. (B, D) All strains except those with no net OD_{660} increase (Δ*fdxC fdxC* (high), Δ*anfDGK*) were normalized by final OD_{660}. (A-D) Data are from three independent cultures. Error bars represent the standard deviation from the mean. All strains carry an in-frame deletion of Δ*nifD* Δ*modABC* to ensure the expression of Fe-nitrogenase genes (*anf*). *R. capsulatus* strains were grown diazotrophically in an RCV minimal medium under an N_2 atmosphere.

upregulated protein detected in Δ*fdxC*, suggesting it could be important for maintaining Fe-nitrogenase activity in the absence of *fdxC*. Fe-nitrogenase activity was also recovered upon plasmid complementation of *fdxN* in the Δ*fdxN* and Δ*fdxCN R. capsulatus* strains to WT levels and around 70% of the WT, respectively (Fig. 5B and D).

Interestingly, introducing both multiple copies of *fdxN* (high) and a single copy of *fdxN* (single) recovered growth and nitrogenase activity to similar levels. These results showed that the cells tolerated the expression of *fdxN* under the *anfH* promoter and could be used as a starting point for engineering electron flux to the Fe-nitrogenase. The fact that boosting the number of copies of *fdxN* did not increase nitrogenase activity implies that the bottleneck for electron flow to nitrogenase is at a different stage than the final Fd-mediated electron transfer. Other studies have indicated that the bottleneck is perhaps prior to the reduction of Fd. Specifically, it was shown that the upregulation of *rnf* gene expression in *R. capsulatus* resulted in increased Mo-nitrogenase activity (20). Future work could combine the over-expression of the *rnf* genes with the over-expression of *fdxN* to observe if there is increased electron transfer to nitrogenase under these conditions.

Expression of *fdxC* under the *anfH* promoter in Δ*fdxC* and Δ*fdxCN* strains recovered growth and nitrogenase activity but not to WT levels and only when a single copy number plasmid was used (Fig. 6).

Growth and nitrogenase activity were partially recovered when *fdxC* was introduced from a single copy number plasmid into the Δ*fdxC* strain. The doubling time of Δ*fdxC fdxC* (single) was 2 h slower than the WT, increasing from 11 h to 13 h, and nitrogenase activity was only recovered to around 50% of the WT (Fig. 6A and B; Table 3). This observation implies that the genomic context of *fdxC* may be important for functionality.

Perhaps the natural *fprA* promoter coordinates the *fdxC* gene expression with other related genes, such as FprA, which might be necessary for the function of FdC.

Growth and nitrogenase activity were only partly recovered when *fdxC* was introduced from a single copy number plasmid into the double Δ*fdxCN* deletion strain (Fig. 6C and D). Doubling times of Δ*fdxCN fdxC* (single) were half as fast as the WT, at 23 h, and nitrogenase activity was around fourfold less than WT. Both changes in growth and activity were comparable to the Δ*fdxN* deletion strain, which had a similar genotype, being no copies of *fdxN* and one copy of *fdxC*.

Surprisingly, introducing several copies of *fdxC* prevented diazotrophic growth and did not recover nitrogenase activity in both the Δ*fdxC* and Δ*fdxCN* strains. This phenotype was not observed when cultures were grown under ammonium or serine, as the *anfH* promoter was not induced, thus indicating that *fdxC* gene expression was toxic during diazotrophic growth. This toxicity could have been caused by an imbalance in the cellular redox state due to the increased number of FdC proteins per cell. The disruption of stoichiometry to its hypothesized partner protein FprA may have destroyed the cells' ability to grow diazotrophically (53).

The function of FdC remains undetermined, though prior research provides information into what FdC is likely not doing. Specifically, FdC has a high reduction potential of -275 ± 2 mV at pH 7.5 and hence cannot donate electrons to Mo-nitrogenase *in vitro* (53). FdC was suggested to be the physiological electron donor for the N_2 fixation-related flavoprotein FprA, which was also upregulated in the Δ*fdxC* deletion strain, though the role of FprA remains unknown. FdC likely does not act as a direct electron donor to the Fe-nitrogenase but has a different role in the electron transfer pathway. *In vitro* studies with purified FdC and Fe-nitrogenase are necessary to determine the role of FdC.

Overall, our experiments suggest that only FdN and FdC have vital roles in N_2 fixation by the Fe-nitrogenase in *R. capsulatus*. The results imply that there is not a high level of functional redundancy between FdN and FdC and their roles are likely distinct. This conclusion is further supported by key differences between FdN and FdC in terms of protein size, coordinated FeS clusters, and predicted protein structures (Fig. S4; Table 1).

Building on this information, we wanted to investigate what underpins Fd-mediated electron donation to nitrogenases. Hence, we decided to construct a phylogeny of all [Fe_4S_4]-cluster Fds from *R. capsulatus* (Fig. 7), as FdA and FdN are [Fe_4S_4]-cluster Fds known to donate electrons to the Mo-nitrogenase *in vitro* (Table 1) (42, 45). There were three *R. capsulatus* Fds included in the alignment: FdA, FdN, and FdB. Despite also being a N_2 fixation-related Fd, the function of FdB is unknown and FdB is incapable of electron transfer to the Mo-nitrogenase *in vitro* in spite of its similarity to FdA and FdN (43). The phylogenetic reconstruction of [Fe_4S_4]-cluster Fds provided insight into the genealogical relationships between *R. capsulatus* Fds: FdA, FdB, and FdN, and other N_2 fixation-relevant Fds from other model diazotrophs.

As *R. capsulatus* FdN was observed to be important for N_2 fixation by the Fe-nitrogenase, we were interested in whether FdN had sequence similarities to other known electron donors to nitrogenases. We observed that FdN branched within other 2[Fe_4S_4]-cluster binding proteins, specifically FdN had a high similarity to four other known electron donors to nitrogenase, these being *R.s palustris* proteins Fer1 and FdN, the *Sinorhizobium meliloti* protein FdxN and the *Rhodospirillum rubrum* protein FdxN (21, 54, 55). Also clustering on the same side of the tree were YhfL-like Fds, which contain 2[Fe_4S_4]-clusters and are found in many N_2-fixing bacteria (56).

On the other hand, Fds grouping closely to FdA were Fds which bind one [Fe_3S_4]-cluster and one [Fe_4S_4]-cluster. Notably, FdA grouped closely to *A. vinelandii* protein Fer1, known to drive N_2 fixation in combination NifF *in vivo* (57). The branching of FdN and FdA near other known electron donors for nitrogenase further supports that both proteins are relevant for N_2 fixation.

FdB clustered closely to other 2[Fe_4S_4]-cluster binding proteins. Interestingly, FdB fell within the same group as a heterocyst Fd from the cyanobacterium *Anabaena* sp.
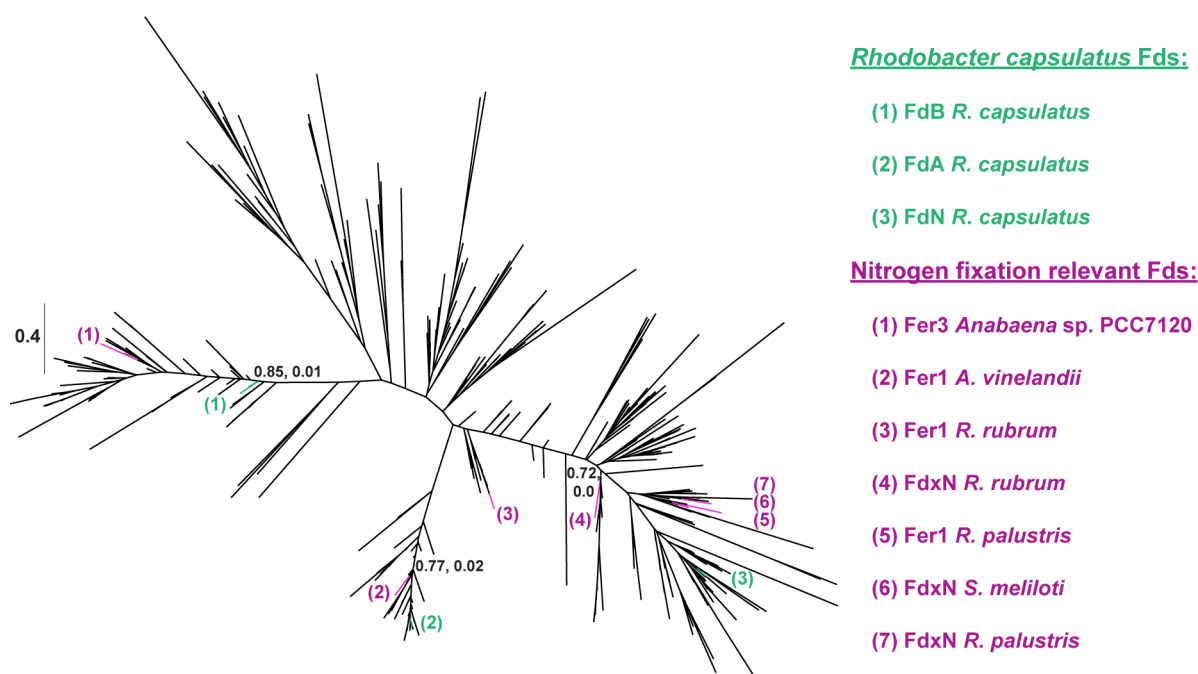
FIG 7 Unrooted phylogenetic tree of [Fe$_4$S$_4$]-cluster containing ferredoxins from *R. capsulatus*. *R. capsulatus* Fd sequences are colored in green and numbered according to the green key on the right. N$_2$ fixation-relevant Fd sequences from other model diazotrophs are colored in purple and numbered according to the purple key on the right. Transfer bootstrap normalized supports (first number) and Felsenstein's Phylogenetic Bootstrap values (second number) of key internal nodes are indicated on the tree.

PCC7120 called Fer3, which is involved but not essential to N$_2$ fixation (58). The phylogenetic reconstruction did not provide any clear clues as to the function of FdB. However, future studies focusing on sequences at the branching point between FdB, FdN, and FdA could give insights into why FdN and FdA can donate electrons to nitrogenases but FdB cannot.

The three [Fe$_2$S$_2$]-cluster Fds (FdC, FdD, and FdE) from *R. capsulatus* were not included in the phylogeny because there are no known electron donors to nitrogenase that harbor only a [Fe$_2$S$_2$] cluster. Moreover, the [Fe$_2$S$_2$]-cluster Fd sequences were too divergent to be included with the [Fe$_4$S$_4$]-cluster Fds in a single phylogeny. Thus, a separate phylogeny of the [Fe$_2$S$_2$]-cluster Fds was created (Fig. S5). Due to the lack of functionally characterized homologs of the *R. capsulatus* [Fe$_2$S$_2$]-cluster Fds, no insightful information could be obtained from this tree.

In summary, the phylogenetic reconstructions showed that even among the [Fe$_4$S$_4$]-cluster binding Fds from *R. capsulatus,* there was significant sequence variation, likely impacting the electrochemical properties of each Fd. Understanding how the biochemistry and biological roles of Fds are impacted by differences in the coordinated metalloclusters and divergent amino acid sequences is critical to understanding these ubiquitous proteins.

DISCUSSION

Our results are the first investigations into the electron transport to the Fe-nitrogenase. Through whole proteome analysis, the most upregulated proteins under N$_2$-fixing conditions by the Fe-nitrogenase were defined and subsequently targeted. Despite deleting the genes for many upregulated soluble charge carriers, only the deletion of *fdxN* or/and *fdxC* disrupted electron transport to the Fe-nitrogenase in *R. capsulatus*. These disruptions were defined by deletion strains growing half as fast diazotrophically and having much lower nitrogenase activity *in vivo*. Proteome analysis of Δ*fdxN* and Δ*fdxC* strains revealed significant upregulation of electron transport proteins, notably

NifF, further indicating a disrupted electron transport. Finally, complementation studies of ΔfdxN and ΔfdxC strains showed distinct patterns for fdxN and fdxC. fdxN complementation successfully recovered WT phenotypes and was tolerated from both high-copy and low-copy number plasmids. Whereas fdxC complementation only partially recovered WT phenotypes, meaning the Fe-nitrogenase activity was not restored to WT levels and fdxC complementation was only tolerated from a single copy number plasmid. The introduction of several fdxC copies was lethal to the R. capsulatus cells under N_2-fixing conditions.

The differences in proteome shifts and complementation patterns between ΔfdxN and ΔfdxC indicated that FdN and FdC likely have different functions. This conclusion is supported by prior electrochemical characterizations, highlighting key differences in reduction potential, Fe-S-cluster identity, and size between FdN and FdC (43, 52). Finally, sequence homology also implied differing functions for FdN and FdC. FdN is more closely related to FdA, the only other Fd shown to donate electrons to the Mo-nitrogenase in vitro. By contrast, FdC is closer related to $[Fe_2S_2]$-cluster Fds, that is, FdD, which is incapable of reducing nitrogenases (42). Future in vitro studies are necessary to characterize electron transfer between Fds and the Fe-nitrogenase. Crucial data, such as comparable reduction potentials and structural data, are required to understand the nature of electron delivery to nitrogenases. Purification of FdN and in vitro assays with the Fe-nitrogenase would reveal if FdN can reduce the Fe-nitrogenase reductase, as observed for the Mo-nitrogenase reductase (45). In vitro studies would also help elucidate the function of FdC, perhaps either in the electron transfer to the reductase component or in cluster maturation and transfer. Characterizing the other proteins within the fprA operon may also help reveal the function of FdC, as FdC may be an electron donor or acceptor to one of these proteins (28).

This research has biotechnological implications. Specifically, characterizing the electron transfer pathway to the Fe-nitrogenase is critical for the in vivo engineering of R. capsulatus for increased gas fixation, either N_2 or CO_2. As the bottleneck for N_2 fixation is believed to be the speed of electron delivery to nitrogenases, electron flux can be altered by targeting Fds, either increasing the number of Fds in vivo or engineering the Fds themselves at possible protein interaction interfaces or the cluster coordination sites. In addition, R. capsulatus is a biotechnologically relevant host as it generates ATP for N_2 fixation via anaerobic photophosphorylation using light as an energy source. Due to the availability of light, R. capsulatus is a suitable host for the development of sustainable biotechnological processes (59). Finally, our research further defined the minimal gene requirements for N_2 fixation, which is vital for research looking to transfer functional nitrogenase systems from diazotrophs into other bacteria or eukaryotes and ultimately plants (60, 61). Future projects will explore the manipulation and optimization of FdN and FdC to increase electron flux to Fe-nitrogenases, improving N_2 and CO_2 conversion.

MATERIALS AND METHODS

Bacterial strains and growth conditions

Chemicals were obtained from Carl Roth (Karlsruhe, Germany) or Tokyo Chemical Industry (Tokyo, Japan), gases from Air Liquide Deutschland GmbH (Düsseldorf, German), enzymes, and E. coli DH5α from New England Biolabs (Ipswich, United States). Sequencing was performed by Microsynth (Balgach, Switzerland).

Rhodobacter capsulatus strains were derivatives of R. capsulatus wild-type strain BS85 (50). R. capsulatus cells were cultured in minimal (RCV) and rich media (PY) according to Katzke et al (62).

Diazotrophic growth conditions were photoheterotrophic: RCV minimal media with 30 mM DL-Malic acid (62), 100% N_2 atmosphere at 0.2 atm at 30°C, and under saturated illumination, by LED panels (9) (420 nm, 470 nm blue lights and 850 nm infrared lights with an output of 12.0 V and light intensity of 80–85 µmol photons m^{-2} s^{-1} per side,

or 160–170 total on samples). Non-nitrogen fixing conditions additionally had 10 mM $(NH_4)_2SO_4$.

Escherichia coli (*E. coli*) strains DH5α were cultured in rich media (LB), with 50 µg/mL kanamycin sulfate, at 37°C and 180 rpm.

R. capsulatus deletion strain construction

Deletion strains were constructed using a *sacB* scarless deletion system (63). Flanking homologous regions to each deletion gene were amplified using PCR with Q5 High-fidelity DNA polymerase and cloned into pK18mob-sacB *via* Golden Gate with BsaI-HF v2. Cloning products were transformed into DH5α and screened *via* blue-white screening using 200 µg/mL XGAL LB-agar plates. Multiple white colonies were sequenced and a single correct clone was stocked.

Deletion plasmids were transformed into ST18 *E. coli* and subsequently conjugated into *R. capsulatus* as described prior (62). *R. capsulatus* strains were passaged aerobically in PY media for several days before growth anaerobically on 5%-sucrose plates. Counter-selection of single colonies was performed and Kan-sensitive colonies were sequenced. Successful deletion strains were sequenced and stocked.

E. coli ST18 cells were grown in the presence of 50 µg/mL kanamycin sulfate and 50 µg/mL 5-aminoleuvelinic acid $C_5H_9NO_3$.

R. capsulatus complementation strain construction

fdx genes were amplified from genomic DNA using PCR with Q5 high-fidelity DNA polymerase. DNA concentrations were determined using a nanodrop (Thermo Scientific, Waltham, United States). PCR fragments were cloned into plasmid *via* Golden Gate with BsaI-HF v2 or Gibson assembly [New England Biolabs, Gibson Assembly Protocol (E5510)]. Cloning products were transformed into DH5α and screened using colony-PCR with DreamTaq polymerase 2× MM. Several promising colonies were sequenced and correct clones were stocked. Expression plasmids were transformed into ST18 *E. coli* and subsequently conjugated into *R. capsulatus* as described prior (62).

The medium/high copy number plasmid used was pOGG024-Km^R (64), with a pBBR1 replication region and kanamycin resistance cassette introduced (15). The single-copy number plasmid was pNMS16, pABC4 replication region, and the kanamycin resistance cassette, donated by Prof. Dr. A. Becker. pOGG024 was a gift from Philip Poole (Addgene plasmid #113991; http://n2t.net/addgene:11991; RRID:Addgene_113991).

Growth behavior of *R. capsulatus* deletion and complementation strains

Pre-cultures of *R. capsulatus* deletion strains were inoculated in RCV media with 10 mM $(NH_4)_2SO_4$ and were grown anaerobically for 24 h. Two pre-cultures of *R. capsulatus* complementation strains were inoculated, the first in RCV media with 10 mM serine and grown anaerobically for 24 h and the second with 1 mM serine for grown anaerobically for 24 h. *R. capsulatus* pre-cultures were washed threetimes in N_2-fixing RCV and OD_{660} was re-measured.

R. capsulatus main cultures, inoculated to OD_{660} 0.02, were grown anaerobically in N_2-fixing RCV media for 5 days. Culture growth was monitored by extracting 100 µL of culture with a nitrogen-flushed needle and OD_{660} was measured using a 96-well plate (Sarstedt AG & Co. KG, Nümbrecht, Germany) and a TECAN Infinite M Nano+ (TECAN, Männedorf, Switzerland). Values were converted to OD_{660} using a calibration factor. The growth of three independent cultures was plotted and doubling times was determined using an exponential (Malthusian) growth model in GraphPad Prism 9.02 for Windows, GraphPad Software, San Diego, California USA.

R. capsulatus deletion strains were grown with 20 µg/mL streptomycin sulfate (Sigma, Darmstadt, Germany) and *R. capsulatus* complementation strains with 50 µg/mL kanamycin sulfate.

Acetylene reduction activity assay

In vivo nitrogenase activity was monitored *via* acetylene reduction. *R. capsulatus* cultures were prepared as stated before; however, after 24 h of diazotrophic growth, 2 mL of each main culture was moved to an empty 20 mL vial in an anaerobic tent (COY Laboratory Products, Grass Lake, United States) under argon atmosphere. The headspace of the vial was exchanged with 90% argon, 10% acetylene, and incubated under illumination for 4 h at 30°C. Assays were quenched using 100 μL 5 M H_2SO_4 (Merck, Rahway, United States). Ethylene and ethane were detected *via* gas chromatography using the gas chromatograph (GC) PerkinElmer Clarus 690 GC (PerkinElmer, Waltham, United States) (15). Raw values were converted to nmol *via* a linear standard curve.

Proteome analysis

R. capsulatus strains were cultured anaerobically until a total OD_{660} of 3 was achieved. Cell samples were prepared by three centrifugation steps and two washing steps with phosphate buffer (3.6 g $Na_2HPO_4 \times 2 H_2O$ and 2.6 g KH_2PO_4 per liter distilled H_2O). For protein extraction frozen cell pellets were re-suspended in 2% sodium lauroyl sarcosinate (SLS) and heated for 15 min at 90°C. Proteins were reduced with 5 mM Tris(2-carboxyethyl) phosphine (Thermo Fischer Scientific) at 90°C for 15 min and alkylated using 10 mM iodoacetamide (Sigma Aldrich) at 20°C for 30 min in the dark. Proteins were precipitated with a sixfold excess of ice-cold acetone, followed by two methanol washing steps. Dried proteins were reconstituted in 0.2% SLS and the amount of proteins was determined by bicinchoninic acid protein assay (Thermo Scientific). For tryptic digestion, 50 μg protein was incubated in 0.5% SLS and 1 μg of trypsin (Serva) at 30°C overnight. Desalted peptides were then analyzed by liquid chromatography-mass spectrometry using an Ultimate 3000 RSLC nano connected to an Exploris 480 mass spectrometer (both Thermo Scientific). Label-free quantification of data -independent acquisition raw data was done using DIA-NN. Further details on sample processing, analytical set up, and bioinformatics analysis are described in the Supplement.

Maximum likelihood phylogeny

Protein sequences for *R. capsulatus fdx* genes were collected from Uniprot. Query sequences were as follows: FdA (>WP_013068498.1), FdB (>WP_013068971.1), FdN (>WP_013068980.1), FdC (>WP_013068981.1), FdD (>WP_013066317.1), and FdE (>WP_013068113.1). Proteins with sequence similarity to individual *R. capsulatus* Fds were identified by performing individual protein-protein searches in BlastP and tBlastn (65). The experimental databases tool was used to limit sequence redundancy and between 40 and 60 sequences were selected from each Fd blast. MUSCLE (66) was used to align each set of Fd-related sequences individually, then against each other, and this total alignment was viewed in AliView (67). The alignment was manually refined to remove lineage-specific insertions. A maximum likelihood phylogenetic tree was generated using RaxmlHPC-AVX.exe v8.2.10 (68) with the PROTGAMMAAUTO, best-scoring models Whelan and Goldman (WAG) or Le and Gascuel (LG), and the Akaike information criterion (aic). The best tree was viewed in FigTree v1.4.4 (69–71). Bootstrap values are TBE normalized supports and Felsenstein's Phylogenetic Bootstrap values generated from 100 replicates.

AUTHOR AFFILIATIONS

[1]Microbial Metalloenzymes Research Group, Max Planck Institute for Terrestrial Microbiology, Marburg, Germany
[2]Core Facility for Mass Spectrometry & Proteomics, Max Planck Institute for Terrestrial Microbiology, Marburg, Germany
[3]Evolutionary Biochemistry Research Group, Max Planck Institute for Terrestrial Microbiology, Marburg, Germany
[4]Center for Synthetic Microbiology (SYNMIKRO), Philipps University Marburg, Marburg, Germany

AUTHOR ORCIDs

Holly Addison http://orcid.org/0009-0002-2541-0746
Johannes G. Rebelein http://orcid.org/0000-0003-2560-716X

DATA AVAILABILITY

Raw data for growth experiments, activity assays, phylogenetic trees, and sequence alignments are deposited on Edmond, the Open Research Data Repository of the Max Planck Society for public access. The mass spectrometry proteomics data have been deposited to the ProteomeXchange Consortium via the PRIDE partner repository with the dataset identifier PXD046902.

ADDITIONAL FILES

The following material is available online.

Supplemental Material

Supplemental Material (mBio03314-23-s0001.pdf). Supplemental text, tables, and figures.
Table S2 (mBio03314-23-s0002.xlsx). Whole proteome analysis.
Table S4 (mBio03314-23-s0003.xlsx). Whole proteome analysis.

REFERENCES

1. Dos Santos PC, Fang Z, Mason SW, Setubal JC, Dixon R. 2012. Distribution of nitrogen fixation and nitrogenase-like sequences amongst microbial genomes. BMC Genomics 13:162. https://doi.org/10.1186/1471-2164-13-162

2. Seefeldt LC, Yang Z-Y, Lukoyanov DA, Harris DF, Dean DR, Raugei S, Hoffman BM. 2020. Reduction of substrates by nitrogenases. Chem Rev 120:5082–5106. https://doi.org/10.1021/acs.chemrev.9b00556

3. Bellenger JP, Darnajoux R, Zhang X, Kraepiel AML. 2020. Biological nitrogen fixation by alternative nitrogenases in terrestrial ecosystems: a review. Biogeochemistry 149:53–73. https://doi.org/10.1007/s10533-020-00666-7

4. Einsle O, Rees DC. 2020. Structural enzymology of nitrogenase enzymes. Chem Rev 120:4969–5004. https://doi.org/10.1021/acs.chemrev.0c00067

5. Jasniewski AJ, Lee CC, Ribbe MW, Hu Y. 2020. Reactivity, mechanism, and assembly of the alternative nitrogenases. Chem Rev 120:5107–5157. https://doi.org/10.1021/acs.chemrev.9b00704

6. Ribbe MW, Hu Y, Hodgson KO, Hedman B. 2014. Biosynthesis of nitrogenase metalloclusters. Chem Rev 114:4063–4080. https://doi.org/10.1021/cr400463x

7. Rutledge HL, Tezcan FA. 2020. Electron transfer in nitrogenase. Chem Rev 120:5158–5193. https://doi.org/10.1021/acs.chemrev.9b00663

8. Seefeldt LC, Hoffman BM, Peters JW, Raugei S, Beratan DN, Antony E, Dean DR. 2018. Energy transduction in nitrogenase. Acc Chem Res 51:2179–2186. https://doi.org/10.1021/acs.accounts.8b00112

9. Zheng Y, Harris DF, Yu Z, Fu Y, Poudel S, Ledbetter RN, Fixen KR, Yang Z-Y, Boyd ES, Lidstrom ME, Seefeldt LC, Harwood CS. 2018. A pathway for biological methane production using bacterial iron-only nitrogenase. Nat Microbiol 3:281–286. https://doi.org/10.1038/s41564-017-0091-5

10. Rebelein JG, Hu Y, Ribbe MW. 2014. Differential reduction of CO_2 by molybdenum and vanadium nitrogenases. Angew Chem Int Ed Engl 53:11543–11546. https://doi.org/10.1002/anie.201406863

11. Hu Y, Lee CC, Grosch M, Solomon JB, Weigand W, Ribbe MW. 2023. Enzymatic fischer–tropsch-type reactions. Chem Rev 123:5755–5797. https://doi.org/10.1021/acs.chemrev.2c00612

12. Rebelein JG, Hu Y, Ribbe MW. 2015. Widening the product profile of carbon dioxide reduction by vanadium nitrogenase. Chembiochem 16:1993–1996. https://doi.org/10.1002/cbic.201500305

13. Oehlmann NN, Rebelein JG. 2022. The conversion of carbon monoxide and carbon dioxide by nitrogenases. Chembiochem 23:e202100453. https://doi.org/10.1002/cbic.202100453

14. Oehlmann NN, Schmidt FV, Herzog M, Goldman AL, Rebelein JG. 2023. CO_2 reduction by the iron nitrogenase competes with N_2 fixation under physiological conditions. bioRxiv. https://doi.org/10.1101/2023.11.30.569367

15. Schmidt FV, Schulz L, Zarzycki J, Oehlmann NN, Prinz S, Erb TJ, Rebelein JG. 2023. Structural insights into the iron nitrogenase complex. Nat Struct Mol Biol. https://doi.org/10.1101/2023.05.02.539077

16. Tezcan FA, Kaiser JT, Howard JB, Rees DC. 2015. Structural evidence for asymmetrical nucleotide interactions in nitrogenase. J Am Chem Soc 137:146–149. https://doi.org/10.1021/ja511945e

17. Sippel D, Einsle O. 2017. The structure of vanadium nitrogenase reveals an unusual bridging ligand. Nat Chem Biol 13:956–960. https://doi.org/10.1038/nchembio.2428

18. Spatzal T, Aksoyoglu M, Zhang L, Andrade SLA, Schleicher E, Weber S, Rees DC, Einsle O. 2011. Evidence for interstitial carbon in nitrogenase femo cofactor. Science 334:940. https://doi.org/10.1126/science.1214025

19. Edgren T, Nordlund S. 2004. The fixABCX genes in *Rhodospirillum rubrum* encode a putative membrane complex participating in electron transfer to nitrogenase. J Bacteriol 186:2052–2060. https://doi.org/10.1128/JB.186.7.2052-2060.2004

20. Jeong H-S, Jouanneau Y. 2000. Enhanced nitrogenase activity in strains of rhodobacter capsulatus that overexpress the rnf genes. J Bacteriol 182:1208–1214. https://doi.org/10.1128/JB.182.5.1208-1214.2000

21. Fixen KR, Pal Chowdhury N, Martinez-Perez M, Poudel S, Boyd ES, Harwood CS. 2018. The path of electron transfer to nitrogenase in a phototrophic alpha-proteobacterium. Environ Microbiol 20:2500–2508. https://doi.org/10.1111/1462-2920.14262

22. Jouanneau Y, Meyer C, Naud I, Klipp W. 1995. Characterization of an fdxN mutant of *Rhodobacter capsulatus* indicates that ferredoxin I serves as electron donor to nitrogenase. Biochimica et Biophysica Acta (BBA) - Bioenergetics 1232:33–42. https://doi.org/10.1016/0005-2728(95)00106-X

23. Poudel S, Colman DR, Fixen KR, Ledbetter RN, Zheng Y, Pence N, Seefeldt LC, Peters JW, Harwood CS, Boyd ES. 2018. Electron transfer to nitrogenase in different genomic and metabolic backgrounds. J Bacteriol 200:e00757–00717. https://doi.org/10.1128/JB.00757-17

24. Strnad H, Lapidus A, Paces J, Ulbrich P, Vlcek C, Paces V, Haselkorn R. 2010. Complete genome sequence of the photosynthetic purple nonsulfur bacterium *Rhodobacter capsulatus* SB 1003. J Bacteriol 192:3545–3546. https://doi.org/10.1128/JB.00366-10

25. Setubal JC, dos Santos P, Goldman BS, Ertesvåg H, Espin G, Rubio LM, Valla S, Almeida NF, Balasubramanian D, Cromes L, et al. 2009. Genome sequence of *Azotobacter vinelandii,* an obligate aerobe specialized to support diverse anaerobic metabolic processes. J Bacteriol 191:4534–4545. https://doi.org/10.1128/JB.00504-09

26. Larimer FW, Chain P, Hauser L, Lamerdin J, Malfatti S, Do L, Land ML, Pelletier DA, Beatty JT, Lang AS, Tabita FR, Gibson JL, Hanson TE, Bobst C, Torres JLT y., Peres C, Harrison FH, Gibson J, Harwood CS. 2004. Complete genome sequence of the metabolically versatile photosynthetic bacterium *Rhodopseudomonas palustris*. Nat Biotechnol 22:55–61. https://doi.org/10.1038/nbt923

27. Schmehl M, Jahn A, Meyer zu Vilsendorf A, Hennecke S, Masepohl B, Schuppler M, Marxer M, Oelze J, Klipp W. 1993. Identification of a new class of nitrogen fixation genes in *Rhodobacter capsalatus*: a putative membrane complex involved in electron transport to nitrogenase. Mol Gen Genet 241:602–615. https://doi.org/10.1007/BF00279903

28. Demtröder L, Pfänder Y, Schäkermann S, Bandow JE, Masepohl B. 2019. NifA is the master regulator of both nitrogenase systems in *Rhodobacter capsulatu*s. Microbiologyopen 8:e921. https://doi.org/10.1002/mbo3.921

29. Buckel W, Thauer RK. 2018. Flavin-based electron bifurcation, ferredoxin, flavodoxin, and anaerobic respiration with protons (Ech) or NAD+ (Rnf) as electron acceptors: a historical review. Front Microbiol 9:401. https://doi.org/10.3389/fmicb.2018.00401

30. Tichi MA, Meijer WG, Tabita FR. 2001. Complex I and its involvement in redox homeostasis and carbon and nitrogen metabolism in *Rhodobacter capsulatus*. J Bacteriol 183:7285–7294. https://doi.org/10.1128/JB.183.24.7285-7294.2001

31. Yakunin AF, Hallenbeck PC. 1998. Purification and characterization of pyruvate oxidoreductase from the photosynthetic bacterium *Rhodobacter capsulatus*. Biochim Biophys Acta 1409:39–49. https://doi.org/10.1016/s0005-2728(98)00145-5

32. Shah VK, Stacey G, Brill WJ. 1983. Electron transport to nitrogenase. purification and characterization of pyruvate:flavodoxin oxidoreductase. J Biol Chem 258:12064–12068.

33. Elsen S, Dischert W, Colbeau A, Bauer CE. 2000. Expression of uptake hydrogenase and molybdenum nitrogenase in *Rhodobacter capsulatus* is Coregulated by the Regb-Rega two-component regulatory system. J Bacteriol 182:2831–2837. https://doi.org/10.1128/JB.182.10.2831-2837.2000

34. Cauvin B, Colbeau A, Vignais PM. 1991. The Hydrogenase structural operon in *Rhodobacter capsulatus* contains a third gene, hupM, necessary for the formation of a physiologically competent hydrogenase. Mol Microbiol 5:2519–2527. https://doi.org/10.1111/j.1365-2958.1991.tb02098.x

35. Meyer J, Kelley BC, Vignais PM. 1978. Nitrogen fixation and hydrogen metabolism in photosynthetic bacteria. Biochimie 60:245–260. https://doi.org/10.1016/s0300-9084(78)80821-9

36. Vignais PM. 2009. Regulation of hydrogenase gene expression, p 743–757. In Hunter CN, Daldal F, Thurnauer MC, Beatty JT (ed), The purple phototrophic bacteria. Springer Netherlands, Dordrecht.

37. Gu W, Milton RD. 2020. Natural and engineered electron transfer of nitrogenase. Chemistry 2:322–346. https://doi.org/10.3390/chemistry2020021

38. Chowdhury NB, Alsiyabi A, Saha R. 2022. Characterizing the interplay of rubisco and nitrogenase enzymes in anaerobic-photoheterotrophically grown *Rhodopseudomonas palustris* CGA009 through a genome-scale

metabolic and expression model. Microbiol Spectr 10:e0146322. https://doi.org/10.1128/spectrum.01463-22

39. Gennaro G, Hübner P, Sandmeier U, Yakunin AF, Hallenbeck PC. 1996. Cloning, characterization, and regulation of nifF from *Rhodobacter capsulatus*. J Bacteriol 178:3949–3952. https://doi.org/10.1128/jb.178.13.3949-3952.1996

40. Armengaud J, Meyer C, Jouanneau Y. 1997. A [2Fe-2S] ferredoxin (FdVI) is essential for growth of the photosynthetic bacterium *Rhodobacter capsulatus*. J Bacteriol 179:3304–3309. https://doi.org/10.1128/jb.179.10.3304-3309.1997

41. Saeki K, Suetsugu Y, Tokuda K, Miyatake Y, Young DA, Marrs BL, Matsubara H. 1991. Genetic analysis of functional differences among distinct ferredoxins in *Rhodobacter capsulatus*. J Biol Chem 266:12889–12895.

42. Yakunin AF, Gogotov IN. 1983. Properties and regulation of synthesis of two ferredoxins from *Rhodopseudomonas capsulata*. Biochimica et Biophysica Acta (BBA) - Bioenergetics 725:298–308. https://doi.org/10.1016/0005-2728(83)90203-7

43. Jouanneau Y, Meyer C, Gaillard J, Forest E, Gagnon J. 1993. Purification and characterization of a novel dimeric ferredoxin (FdIII) from *Rhodobacter capsulatus*. J Biol Chem 268:10636–10644.

44. Armengaud J, Meyer C, Jouanneau Y. 1994. Recombinant expression of the fdxD gene of *Rhodobacter capsulatus* and characterization of its product, a [2Fe-2S] ferredoxin. Biochem J 300 (Pt 2):413–418. https://doi.org/10.1042/bj3000413

45. Hallenbeck PC, Jouanneau Y, Vignais PM. 1982. Purification and molecular properties of a soluble ferredoxin from *Rhodopseudomonas capsulata*. Biochimica et Biophysica Acta (BBA) - Bioenergetics 681:168–176. https://doi.org/10.1016/0005-2728(82)90020-2

46. Yakunin AF, Gennaro G, Hallenbeck PC. 1993. Purification and properties of a nif-specific flavodoxin from the photosynthetic bacterium *Rhodobacter capsulatus*. J Bacteriol 175:6775–6780. https://doi.org/10.1128/jb.175.21.6775-6780.1993

47. Grabau C, Schatt E, Jouanneau Y, Vignais PM. 1991. A new [2Fe-2S] ferredoxin from *Rhodobacter capsulatus*. coexpression with a 2[4Fe-4S] ferredoxin in *Escherichia coli*. J Biol Chem 266:3294–3299.

48. Yoch DC, Whiting GJ. 1986. Evidence for NH_4^+ switch-off regulation of nitrogenase activity by bacteria in salt Marsh sediments and roots of the grass spartina alterniflora. Appl Environ Microbiol 51:143–149. https://doi.org/10.1128/aem.51.1.143-149.1986

49. Saeki K, Tokuda K -i., Fukuyama K, Matsubara H, Nadanami K, Go M, Itoh S. 1996. Site-specific mutagenesis of *Rhodobacter capsulatus* ferredoxin I, FdxN, that functions in nitrogen fixation: ROLE OF EXTRA RESIDUES. J Biol Chem 271:31399–31406. https://doi.org/10.1074/jbc.271.49.31399

50. Hoffmann M-C, Müller A, Fehringer M, Pfänder Y, Narberhaus F, Masepohl B. 2014. Coordinated expression of fdxD and molybdenum nitrogenase genes promotes nitrogen fixation by *Rhodobacter capsulatus* in the presence of oxygen. J Bacteriol 196:633–640. https://doi.org/10.1128/JB.01235-13

51. Hallenbeck PC, Gennaro G. 1998. Stopped-flow kinetic studies of low potential electron carriers of the photosynthetic bacterium, *Rhodobacter capsulatus*: ferredoxin I and NifF. Biochimica et Biophysica Acta (BBA) - Bioenergetics 1365:435–442. https://doi.org/10.1016/S0005-2728(98)00096-6

52. Naud I, Meyer C, David L, Breton J, Gaillard J, Jouanneau Y. 1996. Identification of residues of *Rhodobacter capsulatus* ferredoxin I important for its interaction with nitrogenase. Eur J Biochem 237:399–405. https://doi.org/10.1111/j.1432-1033.1996.0399k.x

53. Jouanneau Y, Meyer C, Asso M, Guigliarelli B, Willison JC. 2000. Characterization of a Nif-regulated flavoprotein (FprA) from *Rhodobacter capsulatus*. European J Bio 267:780–787. https://doi.org/10.1046/j.1432-1327.2000.01056.x

54. Klipp W, Reiländer H, Schlüter A, Krey R, Pühler A. 1989. The *Rhizobium meliloti* fdxN gene encoding a ferredoxin-like protein is necessary for

nitrogen fixation and is cotranscribed with nifA and nifB. Mol Gen Genet 216:293–302. https://doi.org/10.1007/BF00334368

55. Edgren T, Nordlund S. 2006. Two pathways of electron transport to nitrogenase in *Rhodospirillum rubrum*: the major pathway is dependent on the fix gene products. FEMS Microbiol Lett 260:30–35. https://doi.org/10.1111/j.1574-6968.2006.00297.x

56. Benoit SL, Agudelo S, Maier RJ. 2021. A two-hybrid system reveals previously uncharacterized protein-protein interactions within the *Helicobacter pylori* NIF iron-sulfur maturation system. Sci Rep 11:10794. https://doi.org/10.1038/s41598-021-90003-1

57. Martin AE, Burgess BK, Iismaa SE, Smartt CT, Jacobson MR, Dean DR. 1989. Construction and characterization of an *Azotobacter vinelandii* strain with mutations in the genes encoding flavodoxin and ferredoxin I. J Bacteriol 171:3162–3167. https://doi.org/10.1128/jb.171.6.3162-3167.1989

58. Bothe H, Schmitz O, Yates MG, Newton WE. 2010. Nitrogen fixation and hydrogen metabolism in cyanobacteria. Microbiol Mol Biol Rev 74:529–551. https://doi.org/10.1128/MMBR.00033-10

59. Frigaard NU. 2016. Anaerobes in biotechnology, p 139–154. In Hatti-Kaul R, Mamo G, Mattiasson B (ed), Biotechnology of Anoxygenic Phototrophic bacteria. Springer International Publishing, Cham.

60. Tatemichi Y, Nakahara T, Ueda M, Kuroda K. 2021. Construction of recombinant *Escherichia coli* producing nitrogenase-related proteins from *Azotobacter vinelandii*. Biosci Biotechnol Biochem 85:2209–2216. https://doi.org/10.1093/bbb/zbab144

61. Baysal C, Burén S, He W, Jiang X, Capell T, Rubio LM, Christou P. 2022. Functional expression of the nitrogenase Fe protein in transgenic rice. Commun Biol 5:1006. https://doi.org/10.1038/s42003-022-03921-9

62. Katzke N, Bergmann R, Jaeger KE, Drepper T. 2012. Heterologous high-level gene expression in the photosynthetic bacterium *Rhodobacter capsulatus*, p 251–269. In Lorence A (ed), Recombinant gene expression. Humana Press, Totowa, NJ.

63. Schäfer A, Tauch A, Jäger W, Kalinowski J, Thierbach G, Pühler A. 1994. Small mobilizable multi-purpose cloning vectors derived from the *Escherichia coli* plasmids pK18 and pK19: selection of defined deletions in the chromosome of *Corynebacterium glutamicum*. Gene 145:69–73. https://doi.org/10.1016/0378-1119(94)90324-7

64. Geddes BA, Mendoza-Suárez MA, Poole PS. 2018. A bacterial expression vector archive (BEVA) for flexible modular assembly of golden gate-compatible vectors. Front Microbiol 9:3345. https://doi.org/10.3389/fmicb.2018.03345

65. Altschul SF, Gish W, Miller W, Myers EW, Lipman DJ. 1990. Basic local alignment search tool. J Mol Biol 215:403–410. https://doi.org/10.1016/S0022-2836(05)80360-2

66. Edgar RC. 2004. MUSCLE: multiple sequence alignment with high accuracy and high throughput. Nucleic Acids Res 32:1792–1797. https://doi.org/10.1093/nar/gkh340

67. Larsson A. 2014. AliView: a fast and lightweight alignment viewer and editor for large datasets. Bioinformatics 30:3276–3278. https://doi.org/10.1093/bioinformatics/btu531

68. Stamatakis A. 2014. RAxML version 8: a tool for phylogenetic analysis and post-analysis of large phylogenies. Bioinformatics 30:1312–1313. https://doi.org/10.1093/bioinformatics/btu033

69. Rambaut A. 2018. Figtree V1.4.4. http://tree.bio.ed.ac.uk/software/figtree/

70. Whelan S, Goldman N. 2001. A general empirical model of protein evolution derived from multiple protein families using a maximum-likelihood approach. Mol Biol Evol 18:691–699. https://doi.org/10.1093/oxfordjournals.molbev.a003851

71. Le SQ, Gascuel O. 2008. An improved general amino acid replacement matrix. Mol Biol Evol 25:1307–1320. https://doi.org/10.1093/molbev/msn067